RESEARCH ARTICLE | SEPTEMBER 06 2024

## Coherent mode and turbulence measurements with a fast camera $\Theta$

Special Collection: Proceedings of the 25th Topical Conference on High-Temperature Plasma Diagnostics

Gustavo E. Bartolo ■ (D); Sonu Yadav (D); Chloelle Fitz; Earl E. Scime (D)



Rev. Sci. Instrum. 95, 093511 (2024) https://doi.org/10.1063/5.0219330

A CHORUS





#### Articles You May Be Interested In

Alfvénic modes excited by the kink instability in PHASMA

Phys. Plasmas (March 2021)

Fast photodiode arrays for high frequency fluctuation measurements of reconnecting flux ropes

Rev. Sci. Instrum. (September 2024)

Electron-only reconnection and associated electron heating and acceleration in PHASMA

Phys. Plasmas (March 2022)





# 03 July 2025 14:27:41

### Coherent mode and turbulence measurements with a fast camera

Cite as: Rev. Sci. Instrum. 95, 093511 (2024); doi: 10.1063/5.0219330

Submitted: 16 May 2024 • Accepted: 12 August 2024 •

**Published Online: 6 September 2024** 











Gustavo E. Bartolo, Donu Yadav, Chloelle Fitz, and Earl E. Scime



#### **AFFILIATIONS**

Department of Physics and Astronomy, West Virginia University, Morgantown, West Virginia 26505, USA

Note: This paper is part of the Special Topic on Proceedings of the 25th Topical Conference on High-Temperature Plasma Diagnostics.

a) Author to whom correspondence should be addressed: geb00019@mail.wvu.edu

#### **ABSTRACT**

This study employs a fast camera with frame rates up to 900,000 fps to measure the transfer of energy across spatial scales in helicon source plasmas and during flux rope mergers and the measurement of azimuthal mode structures in helicon plasmas. By extracting pixel-scale dispersion relations and power spectral density (PSD) measurements, we measure the details of turbulent wave modes and energy distribution across a broad range of spatial scales within the plasma. We confirm the presence of drift waves in helicon plasmas, as well as the existence of strong dissipation regions in the PSD at electron skin depth scales for both helicon and flux rope merger experiments. This approach overcomes many limitations of conventional probes, providing high spatial and temporal resolution, without perturbing the plasma.

Published under an exclusive license by AIP Publishing. https://doi.org/10.1063/5.0219330

#### I. INTRODUCTION

Plasma phenomena play key roles in a wide range of physical systems, e.g., astrophysical structures, plasma processing, and controlled fusion energy. The flow of energy and momentum in plasmas is often investigated through measurements of fluctuation dispersion relations (to identify waves and instabilities) and through power spectral density (PSD) analysis (to understand the transfer of energy and momentum between different spatial scales). Dispersion relation and power spectral density measurements are traditionally accomplished with in situ probes and recently with two-point optical measurements.

Probe-based measurements perturb the plasma, have limited spatial extent, and face physical constraints on resolvable frequencies. This study explores an imaging technique employing a fast camera for the extraction of pixel-scale radial and azimuthal mode structures in a helicon plasma and power spectral density measurements in a helicon plasma and during the merger of two flux ropes.

The dispersion relation of a wave, which defines the relationship between its frequency (energy) and wavenumber (momentum), uniquely characterizes wave behaviors in a plasma system.<sup>3</sup> Observing specific dispersion relations, such as those of drift waves, indicates that density gradients are driving plasma fluctuations.

Fast imaging facilitates the non-intrusive determination of twodimensional wave mode structures by extracting pixel-scale dispersion relations. According to Taylor's hypothesis, in environments lacking significant mean flow, the lifetime of turbulent eddies,  $\tau$ , is proportional to l/v, where l is the turbulent length scale and vis the mean flow.<sup>5</sup> Thus, the smallest scales of turbulence occur at the highest frequencies. Consequently, capturing these dynamics requires cameras capable of high frame rates to accurately measure fluctuations at large wavenumbers.

Modern cameras allow for detailed observation of transient phenomena at frame rates in excess of 1 000 000 fps. For example, Vincent's studies<sup>6</sup> of eigenmode structures in RF-generated plasmas used fast camera imaging to identify ion acoustic waves through measurements of the mode number vs frequency and comparison with theoretical predictions.

The Power Spectral Density (PSD) provides insight into the energy cascade across spatial scales by transforming turbulent flow data into power per wavenumber,  $S(\mathbf{k},t)$ . PSD analysis of in situ measurements from the Parker Solar Probe (PSP) in the inner heliosphere has identified coronal heating mechanisms and wave-particle interactions, such as ion cyclotron heating, with spectral indices as steep as  $k^{-4}$  at dissipation scales.<sup>7</sup> Similarly, in the Controlled Shear Decorrelation eXperiment (CSDX), Light et al. detected coherent drift waves in an argon plasma column and analyzed their

spectral properties through high-speed digital camera imaging of Ar II line emission. Using cross-spectral phase techniques, they visualized dominant coherent structures across a wide frequency range, identifying them as coherent drift modes. The experimental observations matched theoretical dispersion curves for drift waves after correcting for Doppler shifts. Subsequent CSDX experiments compared coherency of fluctuations observed with probes and imaging, determining that imaged fluctuations were likely due to fluctuations in density and electron temperature. Although the PSD was not reported, electrostatic probes with a 5 mm separation yielded a wavenumber range of  $k_{\min} = 3.49$  rad/m to  $k_{\max} = 628$  rad/m, spanning two orders of magnitude in k.

In these experiments, we demonstrate an initial k measurement range of  $9.1 \times 10^{1}$  to  $2.4 \times 10^{4}$  rad/m for helicon measurements and  $3.5 \times 10^{1}$  to  $2.2 \times 10^{3}$  rad/m for flux rope experiments, a span of roughly two orders of magnitude. We present measurements of the azimuthal mode structure (dispersion relation) in helicon plasmas that corroborate recent studies that found dramatic changes in helicon mode coupling for the reversal of the helicon antenna helicity. 11 We also present measurements of the PSD in helicon and merging flux rope plasmas that show strong evidence of fluctuation dissipation at the electron skin depth scale,  $k_{d,e} = 3.2 \times 10^3$  rad/m and  $k_{d,e}$ =  $3.7 \times 10^3$  rad/m, respectively. The success of this non-intrusive diagnostic method demonstrates its potential as a preferable alternative to conventional probes as it overcomes limitations associated with probe-based measurements, such as concurrent spatial and temporal resolution. Additionally, the spatial resolution ( $\mu$ m/pixel) of these measurements can be refined to an arbitrary level, depending on the quality of the available optics and the photon count. Helicon plasma conditions were argon, with  $n \approx 1 \times 10^{13}$  cm<sup>-3</sup>,  $T_e \approx 3-5$  eV, and  $T_i \approx 0.2-0.5$  eV. Similarly, flux rope plasmas were argon, with  $n \approx 1 \times 10^{13}$  cm<sup>-3</sup>,  $T_e \approx 3$  eV, and  $T_i \approx 0.5$  eV.

The fast camera diagnostic offers high spatial and temporal resolution for studying critical phenomena relevant to fusion and high-temperature plasma, such as turbulence, wave-particle interactions, and magnetic reconnection without perturbing the plasma or endangering the lifetime of diagnostics.

#### II. EXPERIMENTAL APPARATUS

The Photron S9 FastCam records up to 9000 full fps ( $\Delta t$  = 11.1 ms, 1024 × 1024 pixels) and 900 000 partial fps ( $\Delta t$  = 1.11  $\mu$ s, 128 × 16 pixels), with a pixel size of 20 ×20  $\mu$ m² and a CMOS sensor size of 20.48 × 20.48 mm². Images are saved in 12-bit monochrome .mraw format for optimal detail and dynamic range. The helicon plasma measurements utilized 25 000 fps ( $\Delta t$  = 40  $\mu$ s), while the flux rope merger studies captured images at 750 000 fps ( $\Delta t$  = 1.3  $\mu$ s).

For the helicon studies, we used a Minolta AF Zoom lens (1.5 m/4.9 ft Macro,  $\phi$ 55 mm) at 300 mm focal length and f/5.6, attached via a Photodiox pro Sony( $\alpha$ )-Nik and Nik-C adapters to Photron S9. The flux rope studies employed a Tamron SP lens ( $\phi$ 82, 17 mm, f/5.6) with a Nikon-C adapter. The camera's effective fill factor of 94.5% gives an effective focal length of  $FL_{effective} = FL \times 1.495$ , providing spatial resolutions of 189  $\mu$ m/pixel for helicon and 1.41 mm/pixel for flux rope measurements. The camera was positioned 3.4 m from the plasma center to reduce parallax.

The PHAse Space MApping (PHASMA) experiment is designed to investigate space plasma phenomena with non-invasive, volumetric optical diagnostics. For studies of magnetic reconnection in PHASMA, dual plasma guns launch parallel magnetic flux ropes that attract and merge through reconnection. The maximum magnetic field in PHASMA of 2200 G (375 G in the plasma gun region) is created with 22 magnet coils in 6 groups. This flexibility allows for the exploration of plasma dynamics across a diverse collection of magnetic field configurations. Helicon plasmas in PHASMA are created with a  $m=\pm 1$  antenna powered by a 1 kW RF amplifier through a  $\pi$ -matching network. The helicon source operates in either a continuous or pulsed mode across a wide range of antenna frequencies (8–16 MHz). See Fig. 1 for additional details about PHASMA, including directions of camera observations.

All helicon plasma experiments were conducted with a background magnetic field of 1100 G, an antenna frequency of 10.5 MHz, a fill pressure of 3.6 mTorr of argon, with forward RF power of either 400 or 600 W, with <1% reflected power. The magnetic field direction was varied between upstream<sup>+</sup> and upstream<sup>-</sup> configurations (when the magnetic field direction is such that the helical antenna launches m = +1 or m = -1 waves in the upstream direction, respectively). Flux rope merger studies were conducted at gun fill pressures of 15 psi with an axial magnetic field of 150 G.

#### III. THEORETICAL BACKGROUND

The cylindrical geometry of the helicon source naturally lends itself to an assumption of azimuthal symmetry. Before extracting radially dependent azimuthal modes from the measured images, each image frame is decomposed into average and fluctuating components,  $I = \langle I \rangle + \tilde{I}$ , where I is the image intensity,  $\langle I \rangle$  is the time averaged intensity, and  $\tilde{I}$  is the temporally fluctuating intensity, also known as Reynolds decomposition. The temporal average is subtracted from each frame, and the oscillatory component is normalized by the temporal variance. The normalized oscillatory images, transformed into polar coordinates due to the inherent cylindrical symmetry, are represented as  $\tilde{I}(x,y,t) \rightarrow \tilde{I}'(r,\theta,t)$ . These transformed images are utilized to determine dispersion relations. After converting the images to polar coordinates, they are Fourier transformed,

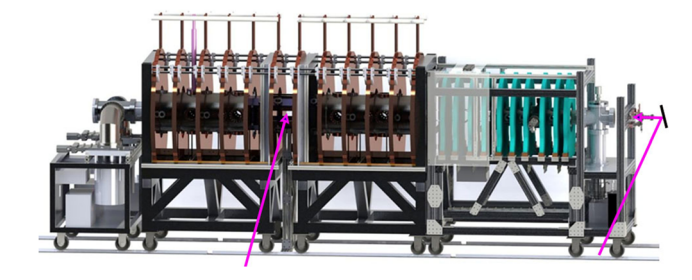


**FIG. 1.** The PHASMA experiment. The water-cooled electromagnets generate an axial magnetic field. The Photron Nova S9 fast camera was placed in two locations for these studies, as shown with magenta arrows. For flux rope studies, the camera viewed the merging flux ropes laterally through a large rectangular port in the middle of PHASMA. For the helicon studies, the camera viewed the plasma from the end through a mirror to reduce the parallax.

$$\hat{I}'(r,m,f) = \int \tilde{I}'(r,\theta,t) e^{-i(m\theta - 2\pi f t)} d\theta dt.$$
 (1)

Here,  $\hat{I}'(r, m, f)$  is the Fourier-transformed oscillatory amplitude, r is the radial position, m is the azimuthal mode number, and f is the temporal frequency.

Computing the norm squared of the Fourier amplitude results in an approximation for the dispersion relation<sup>9</sup> as a function of radius, wavenumber, and frequency,

$$S(r, m, f) = \hat{I}'^*(r, m, f)\hat{I}'(r, m, f).$$
 (2)

The average S(r, m, f) across a range of radii gives an approximation for the polar PSD, S(m, f), for the specific range of radii selected. Equation (2) contains all information necessary to approximate the dispersion relation. Note that this form of the PSD is primarily used to determine the azimuthal mode amplitude (shown in Figs. 2 and 3). By analyzing the peaks or ridges in the S(m, f) plot, one can extract the functional relationship  $\omega = \omega(k)$ .<sup>13</sup> This approach facilitates extracting different dispersion relations for the dense blue core and the outer plasma region in the helicon plasmas.

Whereas with dispersion relation analysis we Fourier transform in space and time, for PSD we simply transform in space, allowing

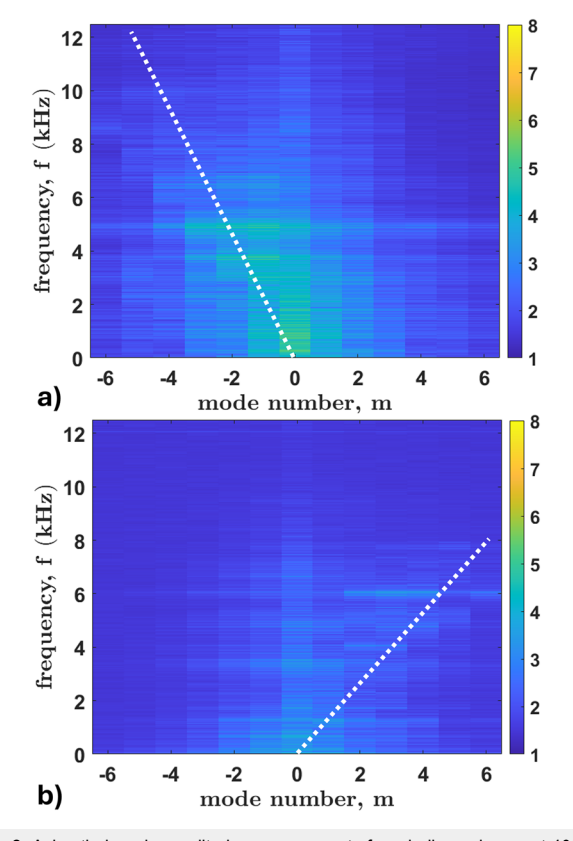


**FIG. 2.** Azimuthal mode amplitude measurements for a helicon plasma at 400 W forward RF power. (a) The upstream $^-$  configuration. (b) The upstream $^+$  configuration. The phase speed of the dominant mode switches sign with the background magnetic field direction (white dashed lines). Both images are integrated over the inner blue core region, within r < 2 cm. Arbitrary amplitude units are in log scale.

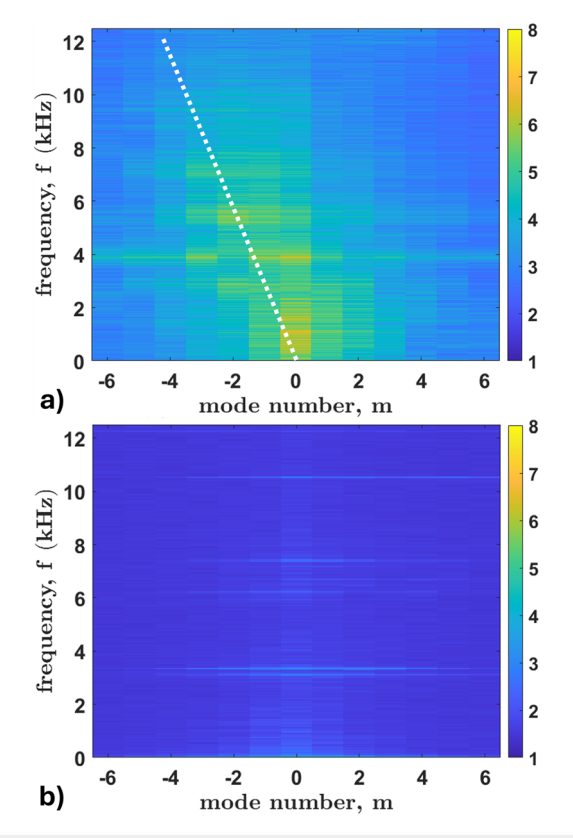


**FIG. 3.** Azimuthal mode amplitude measurements for a helicon plasma at 600 W forward RF power. (a) The upstream $^-$  configuration. (b) The upstream $^+$  configuration. Both images are integrated over the inner blue core region, within r < 2 cm. Arbitrary amplitude units are in log scale.

for temporal resolution. PSD enables the identification of dominant scales of motion and provides insight into the energy transport mechanisms across various spatial and temporal scales. We calculate the FFT of individual frames and convert wavenumber, k, to rad/pixel to rad/m using the determined pixel spatial resolution. The different components of the PSD are determined through the Fourier transform of the auto-correlation function, <sup>14</sup>

$$S_{XY}(k_x, k_y, t) = \frac{1}{N_x N_y} \hat{I}_{XY}^*(k_x, k_y, t) \hat{I}_{XY}(k_x, k_y, t), \tag{3}$$

where  $\hat{I}_{XY}(k_x, k_y, t)$  is the spatial Fourier transform (FFT) of the image,  $k_i$  corresponds to the wavenumber, and  $N_x N_y$  is the total number of pixels for PSD normalization. Note that if a temporal average is well defined, as is the case for helicon studies, Eq. (3) is the stochastic PSD. The stochastic PSD can also be further averaged over all frames, effectively averaging over time. In our work, the averaging range does not significantly affect the resulting PSD.

Equation (3) describes a three-dimensional PSD, which is reduced to fewer dimensions by averaging over one or more coordinate axes. The average radial power spectral density is

$$\langle S_{XY}(k_r,t) \rangle_i = \frac{1}{N} \sum_j S_{XY}(k_x,k_y,t) \delta(k_x^2 + k_y^2 - k_{r,j}^2),$$
 (4)

where  $k_r$  is the radial wavenumber, i is the radial index, and the summation over the PSD occurs at specific radial positions. N, the number of bins summed over, is given by  $N = \sum_i \delta(k_x^2 + k_y^2 - k_{r,i}^2)$ .

This technique then allows for the selective analysis of the PSD based on different spatial dimensions. Specifically, by applying similar methods, we can analyze how the PSD varies depending on the wavenumbers  $k_x$  and  $k_y$  in the x and y directions, respectively. More importantly, by optically zooming into regions of interest, we can observe dynamics at larger wavenumbers—spatial scales that are inaccessible by probes.

#### IV. EXPERIMENTAL RESULTS

Here, we compare our analysis of helicon source images with that of the CSDX experiment,<sup>4</sup> with particular emphasis on the distinctions in mode structures between the inner and outer blue core regions of the plasma. The CSDX studies used an m=0 helicon antenna, which excited  $m=\pm 1$  waves in the plasma core and the plasma edge. In contrast, our experiments used either a m=+1 or a m=-1 antenna configuration. Recent experiments in the PHASMA helicon source reported a significant change in source performance after the reversal of the axial magnetic field, B. Probe measurements of the fluctuating magnetic field components at the antenna frequency indicated that the upstream configuration yields the best density production and an "intense blue core" plasma.

Shown in Figs. 2 and 3 are the amplitudes for each azimuthal mode and frequency obtained from the 2D FFT summed over the inner 2 cm of helicon plasmas in PHASMA for both magnetic field directions and for RF powers of 400 and 600 W, respectively. The FFTs in time use the entire record length, i.e., this analysis method assumes a time-stationary mode structure. For both upstream<sup>-</sup> cases [part (a) of Figs. 2 and 3], there is a relationship between the azimuthal mode number and frequency, i.e., a dispersion relation. When the magnetic field is reversed (the upstream<sup>+</sup> case), the mode structure is much weaker for the 400 W case and essentially vanishes for the 600 W case. These observations are consistent with a significant change in mode structure for different antenna helicities. Perhaps surprisingly, the absence of a clear dispersion relation in the core of the plasma corresponds to the appearance of the bright blue core in the upstream<sup>+</sup> case.

Fitting the mode structure to a linear dispersion relation to calculate the phase velocity,  $V_{\theta} = \omega/k$ , for Figs. 2(a) and 3(a), yields phase velocities of -473 and -413 m/s, respectively. Note that these phase velocity inferences are limited by both the frame rate and the maximum resolvable mode number (dependent on the number of discrete angular steps) up to the Nyquist Frequency. Above m > 6, the mode amplitudes are indistinguishable from noise and are not shown. For the reversed magnetic field case, the phase velocity of the driven modes switches sign, a clear indication that the excited modes are coupled to the helicity of the antenna. <sup>11</sup>

For a classic drift wave, the expected phase velocity is given by  $|\nu_{De}| = \frac{k_B T_e}{e B_0 n_e} \frac{d n_e}{d r}$  and the direction of rotation is in the ion diamagnetic drift direction, i.e., the  $\nabla n \times B$  direction.<sup>3</sup>  $k_B$ . is Boltzmann's constant,  $T_e$  is the electron temperature, and  $n_e$  is the electron density. Using Stevenson's density gradient measurements in the same system, the predicted phase velocity for drift waves is  $V_\theta \sim 600$  m/s,

consistent with the phase speeds inferred here, with potential discrepancy due to unaccounted Doppler shift or errors in the density profile measurements. The negative phase velocity is in the ion diamagnetic drift direction, given the viewing geometry, the direction of the magnetic field for the upstream<sup>-</sup> case, and the direction of the density gradient. Drift waves in the ion diamagnetic direction in the core of the plasma are consistent with observations in CSDX by Light *et al.*<sup>4</sup> and Cui *et al.*<sup>15</sup>

The azimuthal mode amplitudes in each image frame are calculated for annuli from r=0 cm to r=4 cm by recasting each frame into polar bins and then projecting each annulus onto an azimuthal basis set. Then, the angular dependent amplitude for each mode in all the annuli is plotted as a function of time (image frame). Consistent with Figs. 2 and 3, the negative m modes dominate, with the m=-4 mode dominating over the full  $4\times 4$  cm² imaged region. The lower-order m modes penetrate deeper into the plasma core. These observations demonstrate that the phase velocity of the drift waves is strongly coupled to the antenna helicity.

To calculate the PSD in Cartesian wavenumbers, the images are projected according to Eq. (4) and averaged over a finite time interval. Since the entire image is analyzed, spatial resolution is sacrificed to access a much wider range of k values. Welch's method <sup>16</sup> is applied on the power spectrum to smooth out noise, further reducing k resolution. The wider range of k values allows us to look for evidence of dissipation at small spatial scales. Initial testing of this analysis method used the same images obtained for the 600 W helicon case. The power spectrum vs total wavenumber ( $k^2 = k_x^2 + k_y^2$ ) is shown in Fig. 4 for both magnetic field orientations.

The PSD vs wavenumber for a fully turbulent, threedimensional, cascade for wavenumbers smaller than the dissipation scale and larger than the scale at which energy is injected (in the inertial range) is expected to obey a single power law scaling of  $k^{-5/3}$ . The measured PSDs for both magnetic field orientations are clearly not consistent with an inertial range. In the upstream case, the PSD drops by three orders of magnitude at a rate of  $k^{-5.3\pm0.3}$  at the first dissipation feature—suggestive of exceptionally strong damping of fluctuations. The scale at which the PSD spectral index changes dramatically in the upstream<sup>-</sup> case is roughly  $1.53 \times 10^3$  rad/m. For these plasma conditions, the electron skin depth scale occurs at  $k_{d,e}$ =  $3.2 \times 10^3$  rad/m and the ion cyclotron scale is  $k_{d,e} = 1.5 \times 10^3$  rad/m. Strong dissipation of the injected RF wave energy in helicon sources at the electron skin depth based on energetic electron measurements was suggested in recent work by Aguirre et al. 17 In the upstream+ case, the  $k^{-4.0\pm0.3}$  decrease in the PSD occurs over a smaller range of spatial scales, and there is a feature around 300 rad/m that is suggestive of larger scale fluctuations of coupling energy into the plasma at a spatial scale of 2 cm, roughly the diameter of the bright blue core that appears in the upstream<sup>+</sup> case.

In both cases, there is a nearly flat region of PSD past the first dissipation feature, suggestive of very little energy transfer across those spatial scales followed by another strong dissipation feature at the highest resolvable wavenumbers. The electron gyroscale is  $k \sim 10^5$  rad/m, just past the resolvable range of wavenumber scales in these measurements.

Given these PSD measurements are based on fluctuations in light emission that might scale as the square of the total fluctuation power (since both density and electron temperature fluctuations

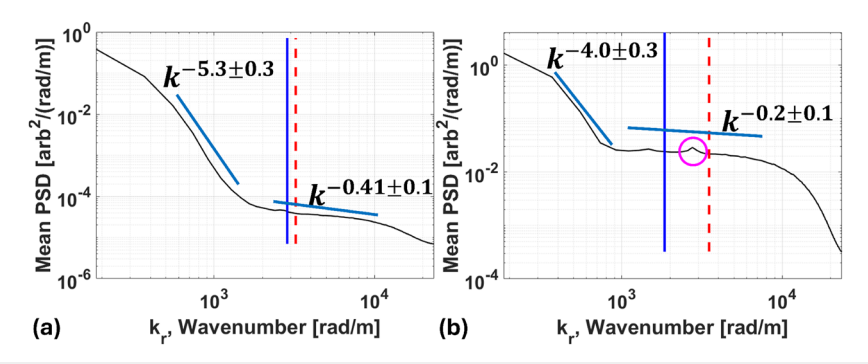


FIG. 4. The time-averaged (over 6.4 s) PSD summed across the entire helicon plasma for the (a) upstream<sup>-</sup> case and (b) the upstream<sup>+</sup> case. The dashed red line is the electron skin depth scale, the solid blue line is the ion cyclotron scale, and a spectral feature is given in magenta. Averaged by applying Welch's method.

contribute to the fluctuations in emission intensity  $^{10}$ ), it is possible that an inertial range cascade should scale as  $k^{-10/3}$ . To properly validate the spectral indices measured through this method will require detailed comparison with probe-based measurements across the same spatial scales and in the same spatial region. Helicons provide an excellent test bed for turbulent plasma experiments, yet these techniques are equally applicable to other turbulent and non-stationary plasma experiments. For instance, consider the merger of two plasma current ropes in a magnetic reconnection experiment.

A typical flux rope merger image is shown in Fig. 5(c). The axes of the ropes are along the y direction and the flux ropes merge along the x direction. In situ magnetic probe measurements find that most of the small-scale reconnection dynamics in PHASMA occurs in the merger direction. Therefore, the camera viewing geometry and resolution were chosen to favor enhanced spatial resolution along the x axis. Since flux rope merger experiments are not steady state, the PSD analysis is conducted at multiple time steps throughout the merger process. The lack of structure along the flux rope axis and the lower resolution of the measurement is reflected in the lack of any features in the  $k_y$  PSD measurements shown in Fig. 5(b). The spectral

index of the  $k_y$  PSD ranges, due to significantly reduced resolution at high frame rates, is unreliable due to spectral leakage.

In the  $k_x$  direction [Fig. 5(a)], there is a region of enhanced PSD around  $k_x \sim 200$  rad/m, which corresponds to the width of the flux ropes and is a natural scale at which energy is injected into the system. Just before the merger, more power appears at flux rope width scale, while the spectral index in the dissipation range stays consistently around  $k_x^{-6.5\pm0.2}$ , where the range is the standard deviation. Once the merger occurs [see Fig. 5(f)], significantly more energy appears in the  $k_x$  PSD at all scales and the spectral index for the decay near 200 rad/m decreases slightly to  $k_x^{-5.8\pm0.2}$ . Note that these features and dissipation regions exist between the electron skin depth scale of  $3.7 \times 10^3$  rad/m and the ion gyroscale of  $2.8 \times 10^2$  rad/m.

These preliminary, image-based PSD measurements reveal significant energy dissipation at electron skin depth scales in electrononly, collisionless magnetic reconnection. These measurements provide important insight into how energy is localized and dissipated at microscopic scales during magnetic reconnection. This study of flux rope mergers show clear evidence for fluctuation energy injection at the flux rope width scale as the merger process initiates.

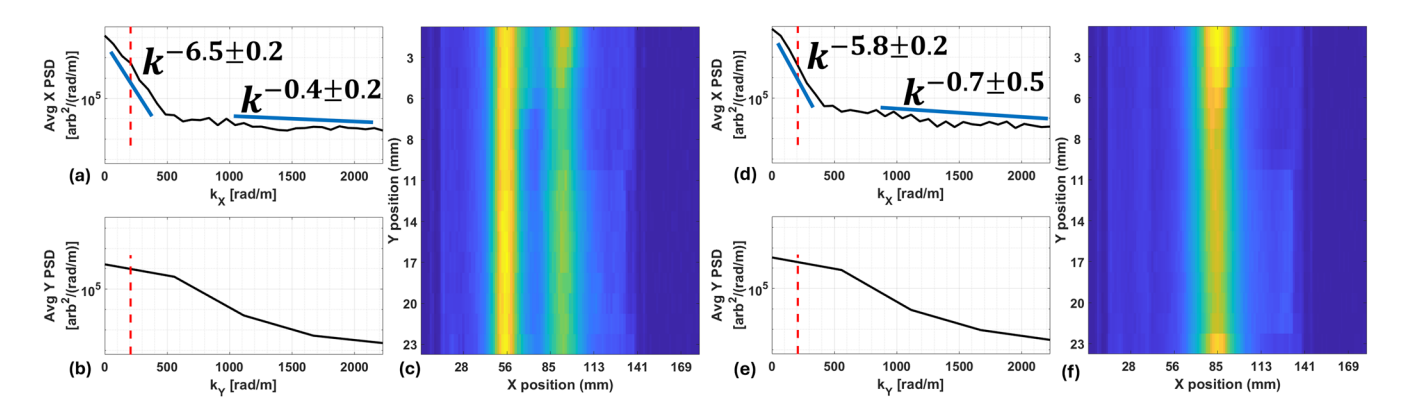


**FIG. 5.** PSD just before and during flux rope merger. (a) The average PSD along x and (b) the average PSD along y, (c) A camera image showing the flux ropes at  $t = 8 \mu s$ . (d) The average PSD along x and (e) the average PSD along y. (f) A camera image showing the flux ropes at  $t = 12 \mu s$ . There is a strong feature at k = 200 rad/m where dissipation increases sharply in the average PSD along x. The red dashed line is the ion cyclotron scale.

#### V. CONCLUSION

These initial studies demonstrate the feasibility of the image-based dispersion relation and power spectral density measurements. These studies were conducted in argon in the helicon source and magnetic reconnection sections of the PHASMA facility. The methods are applicable to any turbulent experiment where non-perturbative measurements are desired. Through image based measurements,  $\sim -400\,$  m/s phase velocity drift waves were identified in the ion diamagnetic direction. The drift waves were identified through the optically measured dispersion relations for helicon plasma at 400 and 600 W RF power. Power spectral density measurements in helicon plasma and flux rope merger experiments showed evidence of strong dissipation at the electron skin depth scale.

#### **ACKNOWLEDGMENTS**

This work was supported by NSF Award No. 1902111 and DoE Award No. DE-SC0020294.

#### **AUTHOR DECLARATIONS**

#### **Conflict of Interest**

The authors have no conflicts to disclose.

#### **Author Contributions**

Gustavo E. Bartolo: Data curation (equal); Formal analysis (lead); Software (lead); Validation (lead); Writing – original draft (lead); Writing – review & editing (equal). Sonu Yadav: Data curation (supporting); Resources (equal); Supervision (lead). Chloelle Fitz: Data curation (supporting); Investigation (supporting); Software (supporting). Earl E. Scime: Conceptualization (lead); Data curation (equal); Funding acquisition (lead); Methodology (supporting); Project administration (lead); Writing – review & editing (equal).

#### **DATA AVAILABILITY**

The data that support the findings of this study are available from the corresponding author upon reasonable request.

#### **REFERENCES**

- <sup>1</sup> J. M. Beall, Y. C. Kim, and E. J. Powers, J. Appl. Phys. **53**, 3933–3940 (1982).
- <sup>2</sup>S. Mattingly and F. Skiff, Phys. Plasmas **25**, 055707 (2018).
- <sup>3</sup>F. F. Chen, *Introduction to Plasma Physics and Controlled Fusion*, 3rd ed. (Plenum Press, 2016).
- <sup>4</sup>A. D. Light, S. C. Thakur, C. Brandt, Y. Sechrest, G. R. Tynan, and T. Munsat, Phys. Plasmas **20**, 082120 (2013).
- <sup>5</sup>J. Mathieu and J. Scott, *An Introduction to Turbulent Flow*, 1st ed. (Cambridge University Press, Cambridge, UK, 2000).
- <sup>6</sup>S. P. H. Vincent, Ph.D. thesis (Université Lyon 1, 2021).
- <sup>7</sup>T. A. Bowen, B. D. G. Chandran, J. Squire, S. D. Bale, D. Duan, K. G. Klein, D. Larson, A. Mallet, M. D. McManus, R. Meyrand, J. L. Verniero, and L. D. Woodham, Phys. Rev. Lett. **129**, 165101 (2022).
- <sup>8</sup>C. Brandt, S. C. Thakur, A. D. Light, J. Negrete, and G. R. Tynan, Phys. Rev. Lett. **113**, 265001 (2014).
- <sup>9</sup> A. D. Light, S. C. Thakur, and G. R. Tynan, Phys. Plasmas 26, 023502 (2019).
- <sup>10</sup>S. Vincent, V. Dolique, and N. Plihon, Phys. Plasmas 29, 032104 (2022).
- <sup>11</sup> K. J. Stevenson, T. J. Gilbert, T. N. Good, M. Paul, P. Shi, R. Nirwan, P. Srivastav, T. E. Steinberger, and E. E. Scime, Plasma Sources Sci. Technol. 33, 045009 (2024).
- <sup>12</sup>P. Shi, P. Srivastav, C. Beatty, R. John, M. Lazo, J. McKee, J. McLaughlin, M. Moran, M. Paul, E. E. Scime, E. E. Scime, D. Thompson, and T. Steinberger, Phys. Plasmas 28, 032101 (2021).
- <sup>13</sup>I. H. Hutchinson, *Principles of Plasma Diagnostics*, 2nd ed. (Cambridge University Press, 2002), Sec. 7, p. 300.
- <sup>14</sup>A. Leon-Garcia, *Probability and Random Processes for Electrical Engineering*, 2nd ed. (Pearson Education, Inc., 1994), Sec. 7, pp. 419–464.
- <sup>15</sup>L. Cui, A. Ashourvan, S. C. Thakur, R. Hong, P. H. Diamond, and G. R. Tynan, Phys. Plasmas 23, 055704 (2016).
- <sup>16</sup>P. D. Welch, "The use of fast Fourier transform for the estimation of power spectra: A method based on time averaging over short, modified periodograms," IEEE Trans. Audio Electroacoust. **15**, 70–73 (1967).
- <sup>17</sup>E. M. Aguirre, R. Bodin, N. Yin, T. N. Good, and E. E. Scime, Phys. Plasmas 27, 123501 (2020).